Novel Airflow Sensor Using Laser Heated Sn-Microsphere Airgap Fiber Fabry–Pérot Interferometer

Cheng-Ling Lee, Chung-Xian Yang, Teng-Yu Liang, and Chao-Tsung Ma

Abstract— We proposed a novel fiber optic hot-wire anemometer based on an Sn metal airgap fiber Fabry–Pérot interferometer (AG-FFPI). An airgap can be naturally formed between the fiber endface and melting Sn metal via overlaying technique. The metal Sn microcavity is directly heated by a 980 nm pumping laser diode (LD) to obtain desired steady-state high temperature (T) of the Sn metal, which exceeds T of the surroundings. Cooling effect on the heated Sn metal by air flowing is converted to optical wavelength blue shifted of interference fringes. Experimental results demonstrate that the proposed Sn metal microcavity AG-FFPI has good performance for airflow measurement and high response to T in the metal Sn. An average sensitivity of about 0.62 nm/(m/s) over the airflow range of 0–10 m/s is achieved with an Sn-microcavity of 9 μm and heated power of 45 mW.

Index Terms— Fiber optic sensor, airgap fiber Fabry–Pérot interferometer, fiber anemometer, airflow sensor, metal.

I. INTRODUCTION

THE development of reliable airflow measurement techniques is significant in various industrial applications and renewable energy conversion systems, e.g., real-time maximum power point tracking control of a wind turbine generator. Although many existing measurement techniques that use anemometers and flow meters have been developed, hot-wire anemometry (HWA) is the preferred approach for airflow sensing due to its various advantages, such as in measuring rapid flows. The measuring mechanism of HWA is based on the heat transfer from sensors to the surrounding environment, and the method is simple and reliable. Therefore, fiber-optic anemometers based on HWA have attracted substantial research interests [1]–[16]. The most common fiber anemometers based on HWA are heated fiber Bragg grating [1]–[11] and long-period grating (LPG) [11], [12]. Other sensing designs, such as fiber optic interferometric types that include the intermodal [13] and Fabry–Pérot interferometers [14]–[16], have been proposed to investigate their high sensitivity to flows. These fiber optic

HWA-based anemometers use metallic (Au or Ag) thin film coatings on fiber devices to absorb the light carried by optical fibers for achieving heating efficiency [2]–[6], [13]. Recently, Liu et al. presented an LPG coated by a thin film with single-wall carbon nanotubes (SWCNTs), which showed excellent absorption in the infrared range and high thermal conductivity for achieving high heating efficiency. The coated thin films absorb the heat from the laser and convert laser light into heat, which subsequently increases the temperature (T) of the fiber grating sensing element. T of the heated-FBGs depends on the wind speed from surrounding environments, which cools the hot FBGs, thereby shifting their spectral resonance peaks. The abovementioned sensing schemes are reliable and efficient, but deposition technique is further required, making the process time consuming. Therefore, cobalt (Co)-doped and high attenuation fibers are used to absorb heating light, which can function as T-related localized sensing elements [1], [7], [8], [10], [16]. The above specific fibers enable great laser heat absorption. The fibers can be written into fiber grating-based devices [1], [7], [8] and Fabry–Pérot cavity-based HWA [16] for wind speed measurements. Recently, we proposed the first hot-polymer fiber Fabry–Pérot interferometer anemometer for sensing airflow. The highly T-sensitive hot polymer cavity was heated with a low-cost chip resistor to achieve the desired steady-state high T of the polymer. The proposed technique is new, but the use of an external heater limits its applications in real-life systems [14]. Therefore, the present study developed a simple Sn-metal microcavity airgap fiber Fabry–Pérot interferometer (AG-FFPI) anemometer that is heated by an in-line laser diode (LD). Through a simple overlaying technique, an airgap at the fiber endface was formed by the Sn metal that is highly heat absorbent. The simple Sn-metal AG-FFPI was applied for T measurement to demonstrate its high T responses [17], [18]. The Sn metal has good absorption in near-infrared light and high thermal conductivity. With these two favorable features, the proposed fiber anemometer has high sensitivity and simple operation. The Sn metal cavity was initially heated using a 980 nm LD to reach a given steady-state T, which was higher than T of the surroundings. When the hot Sn cavity was cooled by the measured wind, the wavelength fringes of the interference spectra shifted accordingly. The cavity became swollen/shrunk with the increase/decrease of T, thereby causing the redshift/blueshift of the interference fringes. As the proposed sensor relies on the measurement of the wavelength shift in response to T changes caused by the airflow, the flow

Fig. 1. (a) Schematic of the proposed AG-FFPI anemometer. (b) Optical micrograph of the Sn microsphere AG-FFPI.
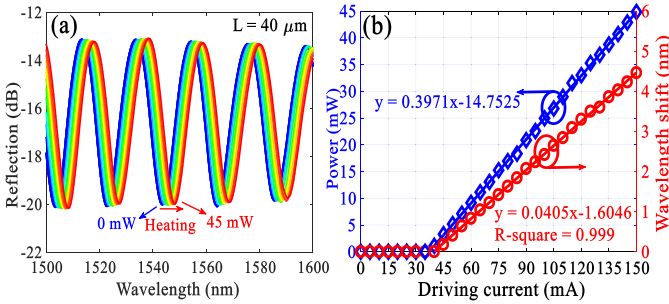
Fig. 2. (a) Spectral responses of the proposed sensor heating by the LD. (b) Driving current corresponding to the LD power for heating Sn-microsphere AG-FFPI (blue line) and wavelength shift displayed in (a), by heating with different powers (red line).

speed can be determined. Experimental results demonstrate that the proposed Sn metal AG-FFPI responds with good sensitivity and high resolution to variations in airflow speed.

II. CONFIGURATION AND OPERATING PRINCIPLES

Figure 1 presents the sensing element of the proposed Sn metal-based airflow sensor. When the fiber endface was carefully inserted into an extremely small drop of melting and shrunk Sn-microsphere, an airgap was formed. The nature phenomenon can be realized the adhesion process between the different kinds of materials. Once a little air is trapped through the adhesion process, an airgap (void) can be readily formed inside the device [19]. The sensor was configured as a simple type of fiber Fabry–Pérot interferometer, and its interferometric mechanism was based on a two-beam interference with low finesse. The Sn metal formed a micro cavity that generates low finesse interference by reflecting from the first and second interfaces. By using the favorable T responsive characteristics of the proposed Sn-metal AG-FFPI, the sensor was initially packaged and heated to high T by an LD with a wavelength of 980 nm through single mode fiber (SMF). The heated Sn metal was cooled by the measured wind, thereby shifting its wavelength fringes. In the test, the proposed fiber airflow sensor was packaged on the thermal insulation plate and the connection of SMF and Sn was fixed with optical glue.

A standard power supply with controllable output current was used to adjust the laser power for achieving the desired steady-state T of the Sn metal with different light powers. Figure 2 displays the responses of the optical spectra heating by the 980nm LD. Figure 2(a) presents the wavelength shift of optical interference fringes with different driving currents (powers) of the heating LD. The microcavity (L)
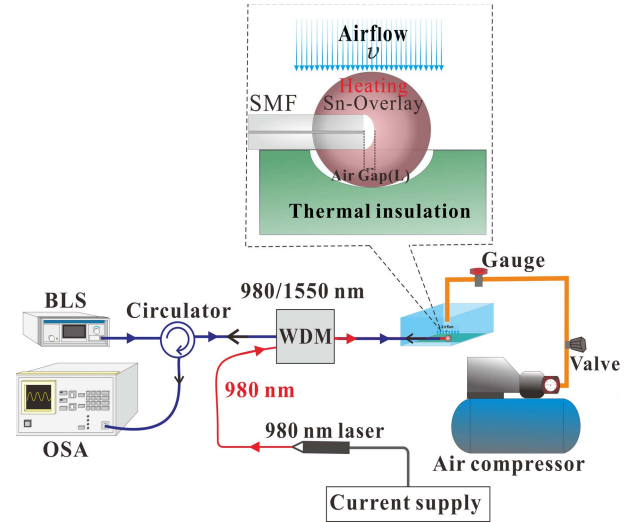
Fig. 3. Experimental setup for measuring the airflow speed. Inset shows the heated Sn-microsphere AG-FFPI.

of the sensor is approximately 40 μm in the heating test. The interference fringes are expected to red-shift (shift to longer wavelength region) with the increase in heating power (P) and T. On the basis of the laser heating results, the heated performance presents highly repeatable responses that are linearly proportional to the heating power (T) with the corresponding power in the range of 0∼45 mW. Figure 2(b) shows the sensitivity of the proposed sensor heating by the laser with variation in P. The threshold current of the LD is approximately 45 mA and relationship of driven current and laser power is shown in the blue line. The optical response of wavelength shift increased immediately when the driven current of LD was higher than 45 mA (red line).

Figure 3 shows the experimental setup for airflow measurements. In this experimental case, a 980 nm pump LD was utilized to heat the Sn microsphere through a 980/1550 nm wavelength division multiplexer (WDM) for the Sn metal to achieve high steady-state T. The sensor was packaged on a specific thermal insulation plastic plate for fixing the junction of the fiber and Sn microsphere. Most parts of the surface of the metal microsphere were exposed to the surrounding for airflow measurement. The measurement system consists of an optical spectrum analyzer (OSA, ADVANTEST-Q8381A), broadband light source (BLS, Opto-Link Corporation Limited OLSWB- OESCLU-FA), and optical circulator. The sensing signal light from BLS propagated to the fabricated AG-FFPI through the WDM, which produces the quasi-sinusoidal interference patterns over a wide range of wavelengths, which can be identified by the OSA. Airflow with different speeds was provided to the AG-FFPI anemometer by an air compressor, which was controlled by a tunable steady flow valve, and its value was monitored by a gauge. For reference, the actual air speed was detected using a commercial hot-wire anemometer, which was located closely to the AG-FFPI probe at the same level. The reflection spectra were individually recorded by OSA when the airflow speed changed, which affected T of the hot Sn metal.
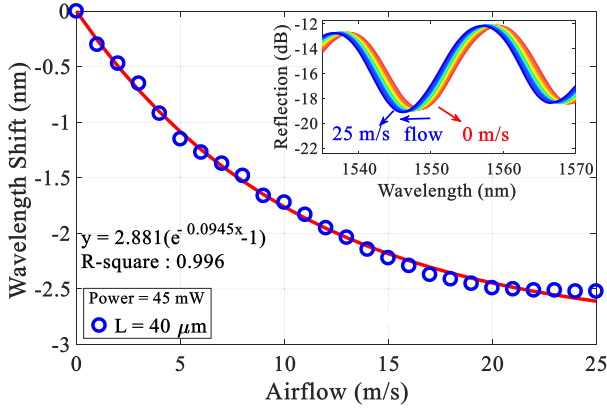
Fig. 4. Wavelength shifts of the interference spectra of AG-FFPI with $L = 40\mu m$ for various airflow speeds.

Fig. 5. (a) Wavelength shifts of interference spectra of $L = 9$ μm AG-FPPI under various airflows in different heating input powers. (b) Sensitivities of the sensor based on Eq. (4) at different heating powers.

III. EXPERIMENTAL RESULTS AND DISCUSSION

By utilizing the valuable high T-responsive characteristics of Sn metal, the proposed sensor is used for airflow measurement to evaluate the effectiveness of the sensing scheme. Initially, the T of AG-FFPI was effectively increased through LD heating before the airflow was measured. Using LD was convenient and fast, thereby keeping the efficiency of the heating process. The air flowed immediately over the surface of the heated Sn metal, thereby reducing its T and blue-shifting the wavelength fringes of the interference spectra. The airflow sensing results shown in Fig. 4 reveal that the airflow cooling reduced T of the Sn metal and shrunk the microcavity of the sensor, thereby blue-shifting the wavelength fringes. The inset of the Fig. 4 shows the detail wavelength shifts ($\Delta\lambda$) in the interference spectra corresponding to the airflow speed (v). The airflow speed at a measurement range of 0–25 m/s was obtained. The experimental results indicated that wavelength shifts vary substantially with the airflow when the speed was below 5 m/s. However, the sensing response weakened at high airflow rates of $v = 20$–25 m/s. The wavelength shifted $\Delta\lambda$ with blue-shifted responses to v, presenting an exponential decay performance. Thus, based on the measured responses, the relationship of $\Delta\lambda$ to v can be simply curve-fitting and expressed as follows:

$$\Delta\lambda = a(e^{bv} - 1). \tag{1}$$

Here, $\Delta\lambda = 0$ nm when $v = 0$ m/s. Sensor configuration with gerater $\Delta\lambda$ at a value of v would have higher sensitivity. In Eq. (1), a and b are the constants of the exponential fitting curve, which are correlated to the sensor sensitivity. The value of a can equivalently represent the total wavelength shift ($\Delta\lambda$) during at a measurement range of 0–25 m/s. Constant b is a negative value that denotes the exponential decay rate to indicate the sensor's sensitivity to v. From Eq. (1), the airflow speed (v) can be easily determined as follows:

$$v = \frac{1}{b}\ln(\frac{\Delta\lambda}{a} + 1). \tag{2}$$

On the basis of Eq. (2), the airflow speed (v) can be estimated when the wavelength shifts ($\Delta\lambda$) of the spectra are measured.
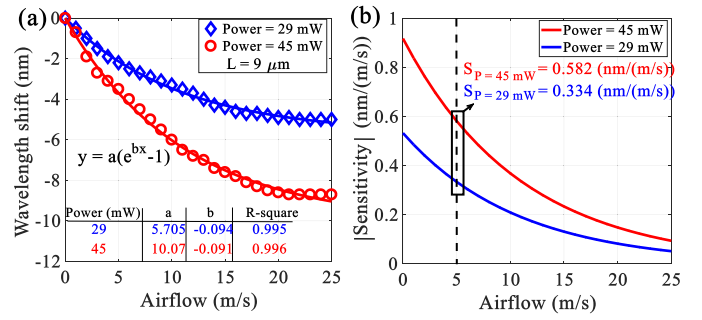
To compare the performances of different heating laser powers (P) affecting the sensing performance, LD heating powers of 29 and 45 mW were used for testing. Figure 5 shows the wavelength shifts of the proposed AG-FFPI anemometer with $L = 9$ μm under different heating powers. Figure 5(a) presents the optical responses of interference fringes to airflow speed (v). The sensing characteristics with exponential fitting constants of a and b for the cases of $P = 29$ and 45 mW are determined in the inset of Fig. 5(a), respectively. Results confirmed that increased T of the Sn metal can achieve improved sensitivity. The exponential decay rate with improved sensitivity of wavelength shift $\Delta\lambda = 2.881(e^{-0.0945v} - 1)$ was obtained when the power was 45 mW.

$\Delta\lambda$ of Eq. (1) can be differentiated to obtain the sensitivity with respect to the flow speed (v), as defined below:

$$S \equiv |\frac{d(\Delta\lambda)}{dv}| \tag{3}$$

Based on the Eq. (3), we can obtain the sensitivities of the proposed Sn metal AG-FFPI anemometer that are strongly correlated with wind speed, as follows:

$$S = Ae^{bv} \tag{4}$$

where constant $A = |ab|$ (a multiplied by b). Here, b is a negative value, thus based on the Eq. (4), A is the highest value at $v = 0$ m/s.

Based on the inset of Fig.5, the A values for the sensors by heating powers of 45 and 29 mW are 0.916 and 0.536 nm/(m/s), respectively. Figure 5(b) shows the sensitivities (S) to flow speed of the proposed sensor based on the Eq. (4) at different heating powers. S values in Fig. 5(b) are presented in red line with high heating power of 45mW, which is higher than that by 29 mW. In the case of $L = 9$ μm, the sensitivities at wind speed $v = 5$ m/s are 0.582 and 0.334 nm/(m/s) for heating powers of 45 and 29 mW, respectively. Figure 6 shows the sensing performances of the proposed Sn metal AG-FFPI anemometers with different cavity lengths (L) with a heating power of 45 mW. Optical wavelength shifts of the measured interferences with L = 9, 40, and 54 μm are presented. The exponential fitting constants a and b for the corresponding cases are shown in the insets of Fig.6(a). In Fig. 6(a), the results demonstrate that a short cavity length provides high sensitivity. The highest exponential
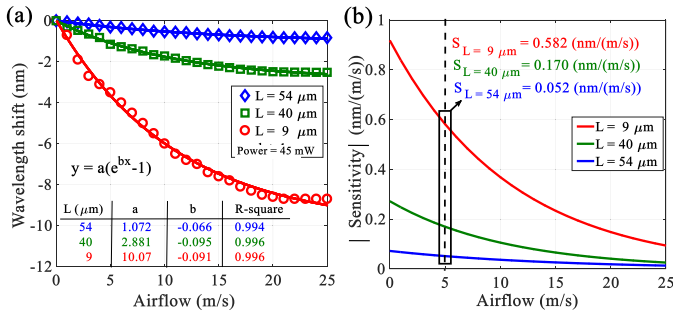
Fig. 6. (a) Wavelength shifts of interference spectra of L=54, 40, and 9 μm AG-FFPIs under various airflows in the same input current. (b) Sensor sensitivity function at interference spectra of 54, 40, and 9 μm.

decay rate with the highest sensitivity of wavelength shift $\Delta\lambda = 10.07(e^{-0.0912v} - 1)$ was obtained in the case of L = 9 μm.

The sensitivity (S) curves to the flow speed of the three sensors with L = 9, 40, and 54 μm are shown in green, red, and blue lines in Fig. 6 (b), respectively. The corresponding sensitivities at wind speed v= 5 m/s are 0.582, 0.170, and 0.052 nm/(m/s) for sensors with L = 9, 40, and 54 μm, respectively. An average sensitivity of 0.62 nm/(m/s) over the airflow range of 0–10 m/s is obtained with an Sn-microcavity of 9 μ and heated power of 45mW. The corresponding resolution of the anemometer was approximately 0.016 m/s when wavelength resolution of OSA is 0.01nm. Furthermore, on the basis of the experimental measured data presented in Figs. 5 and 6, all of the achieved fitting curves of wavelength shifts ($\Delta\lambda$) corresponding to the airflow speed (v) with R-squared value (r^2) are beyond 0.994, which showed the effectiveness of the sensing scheme. The fabrication of the proposed Sn metal microcavity AG-FFPI anemometer and sensing system is small, simple, flexible, and low cost, and it is believed to have great commercial potential.

IV. CONCLUSION

A novel and highly reliable fiber-optic airflow sensor based on an Sn metal AG-FFPI was presented. The designed AG-FFPI-based anemometer with an Sn metal attached to the fiber endface was initially heated by a 980 nm LD with T that exceeded that of the surroundings. The Sn metal was then cooled by the measured flowing air, which greatly shifted the wavelength fringes of its interference spectra due to its high thermal sensitivity. The sensitivity of the proposed anemometer is a function of wind speed. An average sensitivity of 0.62 nm/(m/s) and resolution of 0.016 m/s are achieved with the Sn microcavity of L = 9 μm for wind speed range between 0~10 m/s. Comprehensive experimental results indicated that the proposed hot Sn metal based anemometer can respond sensitively and reliably to variations in airflow speed. This advantage indicates the potential use of such anemometer in various industrial applications with proper design and in the real-time, optimal control and sensing of wind renewable energy conversion systems.

REFERENCES

[1] R. Z. Chen, A. D. Yan, Q. Q. Wang, and K. P. Chen, "Fiber-optic flow sensors for high-temperature environment operation up to 800°C," *Opt. Lett*, vol. 39, no. 13, pp. 3966–3969, 2014.

[2] Z. Yang *et al.*, "Fiber-optic anemometer based on single-walled carbon nanotube coated tilted fiber Bragg grating," *Opt. Express*, vol. 25, no. 20, pp. 24521–24530, 2017.

[3] X. Wang, X. Dong, Y. Zhou, Y. Li, J. Cheng, and Z. Chen, "Optical fiber anemometer using silver-coated fiber Bragg grating and bitaper," *Sens. Actuators A, Phys.*, vol. 214, pp. 230–233, Aug. 2014.

[4] C. Jia, W. Zhu, Z. Huang, and P. Hu, "Experimental and simulation study on thermal gas flowmeter based on fiber Bragg grating coated with silver film," *Sens. Actuators A, Phys.*, vol. 228, pp. 23–27, Jun. 2015.

[5] X. Dong, Y. Zhou, W. Zhou, J. Cheng, and Z. Su, "Compact anemometer using silver-coated fiber Bragg grating," *IEEE Photon. J.*, vol. 4, no. 5, pp. 1381–1386, Oct. 2012.

[6] X. Wang, X. Dong, Y. Zhou, K. Ni, J. Cheng, and Z. M. Chen, "Hot-wire anemometer based on silver-coated fiber Bragg grating assisted by no-core fiber," *IEEE Photon. Technol. Lett.*, vol. 25, no. 24, pp. 2458–2461, Dec. 15, 2013.

[7] L.-H. Cho, C. Lu, A. P. Zhang, and H.-Y. Tam, "Fiber Bragg grating anemometer with reduced pump power-dependency," *IEEE Photon. Technol. Lett.*, vol. 25, no. 24, pp. 2450–2453, Dec. 15, 2013.

[8] S. Gao, A. P. Zhang, H.-Y. Tam, L. H. Cho, and C. Lu, "All-optical fiber anemometer based on laser heated fiber Bragg gratings," *Opt. Express*, vol. 19, no. 11, pp. 10124–10130, May 2011.

[9] J. Wang, Z.-Y. Liu, S. Gao, A. P. Zhang, Y.-H. Shen, and H.-Y. Tam, "Fiber-optic anemometer based on Bragg grating inscribed in metal-filled microstructured optical fiber," *J. Lightw. Technol.*, vol. 34, no. 21, pp. 4884–4889, Nov. 1, 2016.

[10] Z. Li *et al.*, "High sensitivity hot-wire based wind velocity sensor using co-doped fiber and fiber Bragg grating for use in mining applications," *J. Phys.*, vol. 1065, 2018, Art. no. 252023.

[11] P. Caldas *et al.*, "Fiber optic hot-wire flowmeter based on a metallic coated hybrid long period grating/fiber Bragg grating structure," *Appl. Opt.*, vol. 50, no. 17, pp. 2738–2743, 2011.

[12] Z. Liu, F. Wang, Y. Zhang, Z. Jing, and W. Peng, "Low-power-consumption fiber-optic anemometer based on long-period grating with SWCNT coating," *IEEE Sensors J.*, vol. 19, no. 7, pp. 2592–2597, Apr. 2019.

[13] Y. Zhao, H.-F. Hu, D.-J. Bi, and Y. Yang, "Research on the optical fiber gas flowmeters based on intermodal interference," *Opt. Lasers Eng.*, vol. 82, pp. 122–126, Jul. 2016.

[14] C.-L. Lee, K.-W. Liu, S.-H. Luo, M.-S. Wu, and C.-T. Ma, "A hot-polymer fiber Fabry–Pérot interferometer anemometer for sensing airflow," *Sensors*, vol. 17, no. 9, p. 2015, 2017.

[15] G. Liu, W. Hou, W. Qiao, and M. Han, "Fast-response fiber-optic anemometer with temperature self-compensation," *Opt. Express*, vol. 23, no. 10, pp. 13562–13570, 2015.

[16] B. Zhou, H. G. Jiang, C. T. Lu, and S. He, "Hot cavity optical fiber Fabry–Pérot interferometer as a flow sensor with temperature self-calibrated," *J. Lightw. Technol.*, vol. 34, no. 21, pp. 5044–5048, 2016.

[17] C.-L. Lee, C.-H. Hung, C.-M. Li, and Y.-M. You, "Simple air-gap fiber Fabry–Pérot interferometers based on a fiber endface with Sn-microsphere overlay," *Opt. Commun.*, vol. 285, nos. 21–22, pp. 4395–4399, 2012.

[18] C.-L. Lee, W.-F. Liu, Z.-Y. Weng, and F.-C. Hu, "Hybrid AG-FFPI/RLPFG for simultaneously sensing refractive index and temperature," *IEEE Photon. Technol. Lett.*, vol. 23, no. 17, pp. 1231–1233, Sep. 1, 2011.

[19] M. Mukadam, J. Schake, P. Borgesen, and K. Srihari, "Effects of assembly process variables on voiding at a thermal interface," in *Proc. Therm. Thermomech. Phenomena Electron. Syst.*, vol. 1, Jun. 2004, pp. 58–62.